Boston University
Department of Astronomy
725 Commonwealth Avenue
Boston, MA 02215, USA

Phone: (617) 353-3652
FAX: (617) 353-5704
E-mail: bania@buast4.bu.edu

28 January, 1992

NASA FINAL PROJECT REPORT

"IRAS and the Boston University–Arecibo Galactic H I Survey: A Catalog of Cloud Properties"

GODDARD GRANT
IN-89-CR
64308
P-8

Dr. Thomas M. Bania, Principal Investigator

NASA Grant Award No.: NAG 5–1193
Award Period: 1 August 1989 through 31 July 1991

Ms. Maureen Rodgers, Assistant Director
Office of Sponsored Programs, Boston University
25 Buick Street, Boston, MA 02215
(617) 353 – 4365

I. Overview of Project NAG 5–1193

Under this grant award IRAS Galactic Plane Surface Brightness Images were used to identify infrared emission associated with cool, diffuse H I clouds detected by the Boston University–Arecibo Galactic H I Survey. These clouds are associated with galactic star clusters, H II regions, and molecular clouds. Using emission-absorption experiments toward galactic H II regions we determined the H I properties of cool H I clouds seen in absorption against the thermal continuum, including their kinematic distances. Correlations were then made between IRAS sources and these H II regions, thus some of the spatial confusion associated with the IRAS fields near the galactic plane was resolved since the distances to these sources was known. Because we can also correlate the BU–Arecibo clouds with existing CO surveys, these results will allow us to determine the intrinsic properties of the gas (neutral and ionized atomic as well as molecular) and dust for interstellar clouds in the inner Galaxy. For the IRAS-identified H II region sample we have established the far infrared (FIR) luminosities and galactic distribution of these sources.

II. Project Results

One of the primary goals of this project was to determine the far infrared ($\lambda \gtrsim 20\mu m$) properties of a sample of H II regions and the distribution of the luminosities in the Galaxy. These H II regions lie within $\sim 0\overset{\circ}{.}5$ of the galactic plane between longitudes $30° < \ell < 60°$. The IR emission was characterized by the IRAS 60 and 100 μm Super Skyflux images of the galactic plane. The kinematic distances of the H II region sample were taken from emission–absorption experiments conducted as part of the BU-Arecibo Survey. The source list for the H II regions was taken from Lockman's (1989) recombination line survey.

(NASA-CR-189806) IRAS AND THE BOSTON UNIVERSITY ARECIBO GALACTIC H I SURVEY: A CATALOG OF CLOUD PROPERTIES Final Report (Boston Univ.) 8 p CSCL 03A

N92-17695

Unclas
G3/89 0064308

Casual inspection of the Skyflux images of the galactic plane at 60 and 100 μm reveals that H II regions are bright sources embedded in diffuse, extended emission. Since we wished to study the far infrared (FIR) emission emanating only from the H II regions the diffuse emission was extraneous to this investigation and needed to be removed. At high galactic latitudes, cold dust ($T_d \sim 20$K) is responsible for the diffuse emission and is well correlated with H I column density. However, at low galactic latitudes the emission is attributed not only to this cold dust but also to dust in quiescent molecular clouds and star forming molecular complexes. To remove this component, the empirical relation between the diffuse emission and H I column density derived at high latitudes would not prove wholly adequate since, at best, it would remove only the contribution from cold dust emission. Therefore an algorithm had to be developed to remove the contribution of the galactic background.

We have adapted for this task an algorithm which had origininally been applied to IRAS data at high galactic latitudes in order to remove zodiacal emission ($| b | \gtrsim 30\,^\circ$, Laureijs, 1989). The general algorithm generated the backgrounds by removing the contribution of point and small, extended sources from the IRAS images. The largest, measured diameter for the H II region sample sources was $\sim 10'$ and sometimes several sources were in close proximity. The parameters for the algorithm were adjusted to take this into account so that several H II regions in the same field were not treated as extended, background emission. Otherwise the background subtraction might remove some of the emission from the H II regions. The resulting background images were smoothed so that they contain emission structures no smaller than approximately $1\,^\circ$. These backgrounds were subtracted from the Skyflux images, leaving just the small scale structures.

The parameters needed to characterize FIR emission were determined from the background subtracted IRAS images. Since the four IRAS detectors have rather wide bandwidths the image fluxes depend on the spectral energy distribution intrinsic to the emission from the source. The Skyflux images are constructed so that the fluxes have a flat ($F_\nu \propto \nu^{-1}$) spectral response. Thus these images need to be color corrected so that the fluxes reflect the true energy distribution of the H II regions. (Color correction algorithms are discussed in the IRAS Explanatory Supplement §VI.C.3.) The emission from the H II regions was modelled as blackbody thermal emission from a medium of optically thin dust. The color temperatures, T_c, are based on the 60/100 μm flux ratios. Modelling the temperatures from the flux ratios requires knowledge of the emissivity law of the dust, since the (color corrected) flux depends on the functional relationship of the optical depth, τ, with wavelength, λ:

$$F_\lambda = \tau_0 \left(\frac{\lambda}{\lambda_0}\right)^\alpha B_\lambda(T_c), \tag{1}$$

where B is the Planck function. The above equation is based on the assumption of optically thin dust emission.

In the dust models of Cox *et al.*(1986), they showed that the extinction curve for silicate grains followed a λ^{-2} dependency for $\lambda \gtrsim 40\mu$m. These models were able to reproduce the average IR spectrum of the galaxy; thus the value of α was chosen as -2 for this work. The color temperatures derived under this emissivity law are essentially the dust temperatures averaged over the grain size. However, this model presupposes the existence of a single grain population. If there are two grain populations present (e.g., graphite grains along with the silicates), then the color temperature for a two component system lies between the physical temperatures of the two grains:

$$T_{\rm silicate} < T_{\rm c} < T_{\rm graphite}. \tag{2}$$

For optically thin emission, the color temperature is derived from the ratio of 60 to 100 μm emission:

$$\frac{F_{60}}{F_{100}} = \left(\frac{60\mu{\rm m}}{100\mu{\rm m}}\right)^{-2} \frac{B_{60}(T_{\rm c})}{B_{100}(T_{\rm c})}. \tag{3}$$

The background subtracted images were used to calculate the color temperatures of the H II regions. The color corrections to the fluxes were applied when determining $T_{\rm c}$.

Most of H II regions appear clearly defined on the color temperature maps, but some of the H II regions are embedded in extended emission structures. This extended emission most likely is due to the residuals from the background subtraction. (For crowded fields our models underestimated the amount of background emission.) However, most sources appear either circular or elliptical in shape. The peak color temperatures range from 19 to 41 K, with the higher temperatures associated with the W51 complex. These peaks are, for the most part, within one or two arcminutes of the H II region recombination line position. The average peak color temperature for the H II region sample was 32 $\pm$ 4 K.

The optical depth of the dust at 100μm can then be extracted from the color corrected 100μm image:

$$\tau_{100} = F_{100}/B_{100}(T_{\rm c}). \tag{4}$$

In general the optical depths of the H II regions reach a minimum near the peak in the color temperature map of each source. In fact, the $\sim$ 0.025 maximum optical depths occur just outside the peak color temperatures. Interior to the H II regions (defined by their appearance in the temperature maps), optical depths range mostly from 0.001 to 0.015. (However, H II regions associated W43 and W51 have optical depths ranging up to 0.03.)

This decrease in optical depths toward the peak in color temperatures has been reported previously. Snell *et al.* (1989) saw optical depths decrease toward FIR point sources. They examined the FIR emission from molecular clouds, rather than from H II regions. To explain these results Snell *et al.* modelled a two component medium consisting of both cold ($T_{\rm dust} \lesssim 15$ K) and hot ($T_{\rm dust}$ = 35 K) dust. They computed 60 and 100 μm fluxes for this model and then used these fluxes to derive the color temperatures and optical depths as if only one component existed. The models showed that the derived color temperatures approached the temperature of the hot component. The optical depths were consistently underestimated and mostly traced the optical depths of the hot component.

The implication for the present analysis is that our color temperatures and optical depths may only trace the hot dust and any of the dust properties derived from our values will only reflect the properties of the hot component.

We have calculated integrated flux maps based on the derived optical depths and color temperatures:

$$F = \int \tau_{100} \left(\frac{\lambda}{100\mu{\rm m}}\right)^{-2} B_\lambda(T_{\rm c}) d\lambda \tag{5}$$

The above equation is integrated over all wavelengths. Although the dust emissivity law is valid only for $\lambda \gtrsim 40\mu$m, the integrated fluxes should be representative of the hot dust emission since

95% of the integrated flux is contributed by $\lambda \gtrsim 50\mu$m. The luminosities, L, of the H II regions were determined by summing up all of the pixels, F_i, in the area surrounding the position of the temperature peak:

$$L = 4\pi d^2 \Delta\Omega \sum_i F_i, \tag{6}$$

where d is the kinematic distance to the H II region and $\Delta\Omega$ is the solid angle of a single pixel. The area of an H II region was defined by examining the integrated flux maps and interactively drawing boundaries around the H II regions. The boundaries typically were defined down to a level of 0.01 to 0.03 ergs^{-1} cm^{-2} sr^{-1} which is a factor 3 to 5 above the background level determined at $\mid b \mid \gtrsim 2^\circ$. The RMS fluctuations at these latitudes were $\sim 2 \times 10^{-4}$ ergs^{-1}cm^{-2}sr^{-1}. The background levels did not reach zero level intensity mainly due to the residual emission from the background subtraction. Thus the uncertainty in the above summation can be regarded as $\sqrt{N} \times$ background level (~ 0.006 ergs^{-1} cm^{-2} sr^{-1}), where N is the number of pixels comprising the H II region. N ranged from 50 to 400 pixels.

The kinematic distances were determined for 70 H II regions in the first galactic quadrant using H I emission–absorption experiments conducted for the BU-Arecibo Survey (Kuchar and Bania 1990; Kuchar 1992). The sample was narrowed to 48 H II regions because of the proximity of some of the H II regions to other sources. The H II regions removed from the sample are located in confused areas, i.e., they were either nearby or overlapped other IR sources. This included some of the H II regions associated with the W51 complex. For these H II regions, it was difficult to define accurate boundaries for the luminosity determination.

Table 1 lists the luminosities for the sample of 48 H II regions. The galactic coordinates (ℓ, b) for each source give the location of the FIR emission peak determined from the integrated flux maps. Column 4 of the table gives the displacement of this peak from the position of the recombination line measurement (Lockman 1989). The average of this offset is just $1'.5 \pm 1'.0$. The last three columns list the kinematic distance, mean physical diameter (determined from the boundaries drawn on the integrated flux map and the kinematic distance), and FIR luminosity of the H II regions. The kinematic distances have an accuracy of $\sim$20%, and thus contribute the largest uncertainty to the luminosities. The distances are based on the rotation curve determined by Clemens (1986) for $R_0 = 8.5$ kpc, $\Theta_0 = 220$ kpc.

Figure 1 shows a face–on view of the galaxy as seen from the north galactic pole with the positions of the H II regions marked with circles. The size of each circle is proportional to the logarithm of the FIR luminosity. The relative sizes of these circles indicate the luminosities. Luminosites between 10^4 and 10^7 erg s^{-1} are noted in the lower right corner of the figure. The axes are in kiloparsecs and fiducial symbols mark the position of the Sun ($\odot$) and the galactic center (+). Galactic longitudes are marked as well.

It is interesting to compare this figure with a similar figure for molecular gas. Clemens *et al.* (1988) produced such a map based on the Massachusetts–Stony Brook CO Survey (Sanders *et al.* 1986). In fact Figure 9 of that paper compared the distribution of giant radio H II regions with density of the molecular gas. Clemens *et al.* found that this sample was preferentially found in regions of high (i.e., twice the average) H_2 gas density. Their sample included 50 H II regions in the longitude range $8^\circ < \ell < 80^\circ$, with 15 H II regions in the longitude range of this work. Thus we have added 30 more sources for this comparison. Again, the same conclusion can be drawn that the H II regions are associated with the denser molecular gas. Also, the brightest H II regions [$\log(L) > 6$] seem to be associated with the densest gas. It should be noted that these correlations are not a result of using the same galactic rotation curve. The kinematic distances in Kuchar and Bania (1990) and Kuchar (1992), from which the H II region distances are obtained, were determined by H I absorption studies and thus independently of Clemens *et al.* (1988).

References

Beichman, C.A., Neugebauer, G., Habing, H.J., Clegg, P.E., and Chester, T.J. (eds.), *IRAS Catalogs and Atlases Explanatory Supplement*, Washington, D.C., U.S. Government Printing Office. 1984.

Clemens, D. P. 1986, *Ap. J.*, **295**, 422.

Clemens, D. P., Sanders, D. B., and Scoville, N. Z. 1988, *Ap. J.*, **327** 139.

Cox, P., Krügel, E., and Mezger, P. G. 1986, *Astr. Ap.*, **155**, 380.

Infrared Processing and Analysis Center (IPAC) (eds.), *Super–Skyflux Explanatory Supplement*, Washington, D.C., U.S. Government Printing Office. 1992, in preparation.

Laureijs, R. *Infrared Properties of Dust in Interstellar Clouds*, Groningen, Netherlands, University of Groningen, 1989.

Lockman, F.J. 1989, *Ap. J. Suppl.*, **71**, 469.

Sanders, D. B., Clemens, D. P., Scoville, N. Z., and Solomon, P. M. 1985, *Ap. J. Suppl.*, **60**, 1.

Snell R. L., Heyer, M. H., and Schloerb, F. P. 1989, *Ap. J.*, **337**, 739.

III. Project Bibliography

Bania, T. M. and Kuchar, T. A. 1992, *"The Boston University — Arecibo Galactic H I Survey"*, *Ap. J. Suppl.*, in preparation.

Kuchar, T. A. 1990, *"IRAS Correlations with Galactic H II Regions"*, unpublished final report to 1990 USAF-UES Summer Graduate Student Research Program.

Kuchar, T. A. 1992, *"The Boston University–Arecibo Galactic H I Survey"*, Ph.D. Dissertation, Boston University.

Kuchar, T. A. and Bania, T. M. 1990, *"H I Emission-Absorption Experiments Toward Galactic H II Regions"*, *Ap. J.*, **352**, 192.

Kuchar. T. A., and Bania, T. M. 1992, *"Far Infrared Properties of Galactic H II Regions"*, *Ap. J.*, in preparation.

TABLE 1

FIR LUMINOSITIES OF H II REGIONS

Source	ℓ (deg)	b (deg)	θ ($'$)	d_{sun} (kpc)	D (pc)	Luminosity ($L_\odot$)
G30.8−0.0	30.764	−0.043	1.1	5.7	22.4	4.554×10^6
G31.0−0.0	31.016	0.013	3.2	8.0	13.4	4.078×10^5
G31.3+0.1	31.284	0.077	1.3	7.3	21.6	9.398×10^5
G31.6+0.1	31.589	0.104	0.6	6.5	19.2	3.491×10^5
G32.2+0.1	32.138	0.097	2.3	8.2	24.2	4.749×10^5
G32.8+0.2	32.785	0.189	0.7	13.4	52.6	2.346×10^6
G33.1−0.1	33.140	−0.097	0.7	7.1	20.4	5.825×10^5
G33.2−0.0	33.205	−0.006	0.7	7.1	16.3	3.885×10^5
G33.4−0.0	33.429	−0.003	0.7	9.5	42.6	1.910×10^6
G33.9+0.1	33.934	0.109	1.2	7.0	21.8	5.475×10^5
G34.2+0.1	34.261	0.166	1.4	3.3	16.2	7.615×10^5
G35.6−0.5	35.599	−0.530	2.5	3.4	11.1	1.708×10^4
G35.6−0.0	35.591	−0.008	1.7	10.7	31.6	1.815×10^6
G36.3+0.7	36.316	0.729	1.7	4.8	22.0	1.573×10^5
G36.5−0.2	36.448	−0.177	0.6	9.1	38.8	4.997×10^5
G37.4−0.2	37.388	−0.214	1.8	11.2	29.2	6.714×10^5
G37.4−0.1	37.341	−0.051	2.0	10.4	27.1	7.418×10^5
G37.5−0.1	37.528	−0.122	0.8	10.4	30.5	1.311×10^6
G37.6+0.1	37.666	0.118	0.9	6.7	19.3	4.720×10^5
G37.8−0.2	37.760	−0.208	0.5	9.4	27.1	9.344×10^5
G37.9−0.4	37.867	−0.377	1.3	9.7	38.1	1.915×10^6
G38.1−0.0	38.034	−0.047	1.1	9.9	41.7	9.997×10^5
G39.2−0.1	39.278	−0.054	1.5	11.9	42.2	1.367×10^6
G41.1−0.2	41.123	−0.211	1.6	9.1	59.1	2.707×10^6

TABLE 1

cont.

Source	ℓ (deg)	b (deg)	θ ($'$)	d_{sun} (kpc)	D (pc)	Luminosity ($L_\odot$)
G41.2+0.4	41.225	0.384	1.2	4.8	23.6	1.195×10^5
G41.5+0.0	41.535	0.043	1.2	11.6	49.5	8.019×10^5
G42.1−0.6	42.112	−0.625	0.2	4.3	21.0	1.913×10^5
G42.4−0.3	42.425	−0.254	0.7	8.5	30.7	6.264×10^5
G42.6−0.1	42.572	−0.140	0.3	4.5	16.2	1.264×10^5
G43.2+0.0	43.172	0.008	0.4	11.9	85.8	1.523×10^7
G43.9−0.8	43.885	−0.769	1.3	8.8	46.1	4.293×10^5
G44.3+0.1	44.293	0.070	2.5	3.9	20.4	1.587×10^5
G45.1+0.1	45.117	0.117	1.3	8.3	46.3	1.481×10^6
G45.8−0.3	45.822	−0.287	0.2	7.5	29.4	3.564×10^5
G46.5−0.2	46.497	−0.242	0.3	3.8	18.7	1.379×10^5
G48.6+0.0	48.589	−0.001	2.6	10.3	47.2	2.270×10^6
G48.6+0.2	48.652	0.199	1.8	10.6	31.3	6.315×10^5
G49.3−0.3	49.425	−0.321	2.8	7.3	17.9	2.420×10^6
G50.0−0.1	50.019	−0.017	3.5	5.5	21.6	1.305×10^5
G51.4−0.0	51.372	0.007	0.7	4.0	19.7	1.544×10^5
G52.2+0.7	52.264	0.684	3.6	10.2	43.5	7.584×10^5
G52.8+0.3	52.787	0.318	2.3	9.3	27.5	9.414×10^4
G53.2+0.2	53.189	0.140	0.9	9.7	31.7	6.964×10^5
G53.6+0.2	53.644	0.247	0.8	7.5	27.1	3.041×10^5
G54.1−0.1	54.086	−0.069	0.4	6.9	42.8	9.256×10^5
G57.5−0.3	57.554	−0.278	0.8	9.0	41.3	2.494×10^5
G59.5−0.2	59.589	−0.137	4.5	6.3	22.7	2.004×10^5
G59.8+0.2	59.797	0.301	3.9	8.7	31.4	2.345×10^5

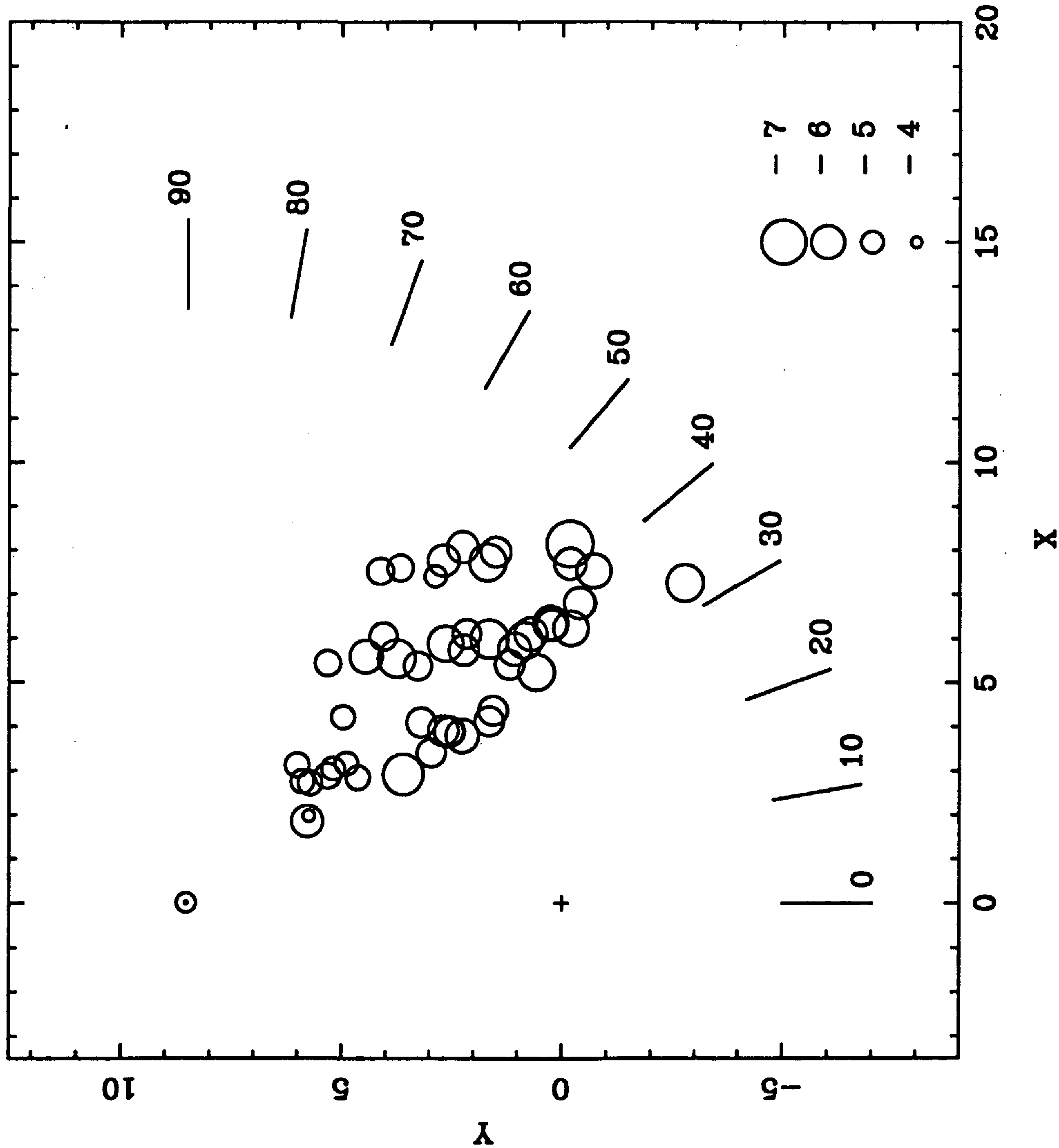
X
Y
0
5
10
15
20
−5
0
5
10
0
10
20
30
40
50
60
70
80
90
7
6
5
4